JOM, Vol. 75, No. 6, 2023
https://doi.org/10.1007/s11837-023-05733-6
© 2023 The Author(s)

TECHNICAL ARTICLE

Study of Solidification Process of Ni-Based Superalloy Castings Manufactured in Industrial Conditions with the Use of Novel Thermal Insulating Module Technique

DARIUSZ SZELIGA ,[1,2,5] MACIEJ MOTYKA,[1,2] WALDEMAR ZIAJA,[1,2] RAFAŁ CYGAN,[3] SYLWESTER FUGLEWICZ,[3] and MAGDALENA GROMADA[4]

1.—Department of Materials Science, Faculty of Mechanical Engineering and Aeronautics, Rzeszow University of Technology, 12, Powstancow Warszawy Avenue, 35-959 Rzeszow, Poland. 2.—Research and Development Laboratory for Aerospace Materials, 4, Żwirki i Wigury Str., 35-036 Rzeszow, Poland. 3.—Investment Casting Division, Consolidated Precision Products, Hetmańska 120, 35-078 Rzeszow, Poland. 4.—Institute of Power Engineering Ceramic Department CEREL, Research Institute, 1 Techniczna St., 36-040 Boguchwała, Poland. 5.—e-mail: dszeliga@prz.edu.pl

The solidification process of IN713C Ni-based superalloy rod castings made by the investment casting method without and with the use of novel insulating module applied on the ceramic mold was studied in this article. The design of the cone-shaped insulating module was developed based on numerical simulations of the distribution of local solidification parameters, ensuring the lowest centerline shrinkage porosity along the castings. The effectiveness of the design of the insulating module was tested in industrial casting trials. It was found that the use of a novel insulation module increases temperature gradient G and decreases cooling rate v, thus leading to a favorable increase of the Niyama criterion value ($Ny = G/\sqrt{v}$) and also ensuring directional solidification of the casting rod compared to the process where thermal insulation was not used. In this way, the centerline shrinkage porosity was removed, maintaining the equiaxed grain structure of the castings. The presented results show that it is possible to use the same insulating module multiple times, in the subsequent manufacturing processes, to control the solidification of Ni-based superalloy precision castings in industrial conditions.

INTRODUCTION

Precision castings of blades and nozzle guide vanes, used in the hot section of gas turbines of aircraft engines, are made of nickel-based superalloys in the investment casting process.[1] In this method, the liquid melt is poured into a preheated ceramic mold in a vacuum furnace. During cooling the melt alloy solidifies inside the mold, and the grain structure and defects are formed, which determine mechanical properties of precision castings.[2,3] Uniform cooling of mold and melt alloy can result in formation of especially dangerous microporosity and centerline shrinkage porosity, caused by insufficient liquid metal feeding into interdendritic channels.[4,5] Proper control of the mold cooling process enables forming of the tapered liquid feeding channel in casting, through which the liquid melt is supplied from gating system to the interdendritic space of moving solidification front, eliminating shrinkage porosity.[2,6] It can be achieved by gradual cooling of consecutive casting volumes using various controlling methods for heat transfer from mold to environment.[2,7–11] For this purpose, in the standard industrial investment casting process, thermal insulation mounted on the mold surface is used. Usually, insulation blankets having different thickness are used as a cover of the external surface of the mold, enabling to control the cooling rate of particular casting volumes.[12] Depending on the

(Received February 23, 2022; accepted January 27, 2023; published online February 23, 2023)

casting complexity, a few blankets can be used as a multi-layer thermal insulation of ceramic mold.[13] This is a time-consuming stage, demanding precise blanked mounting to mold surface or sometimes to another insulation layer, usually by ceramic adhesive. This kind of solidification control is commonly used in investment casting of aircraft engines or gas turbine parts. However, ceramic waste generated after casting productions using disposable molds is a big problem for precision foundries, requiring expensive disposal, especially when insulating blankets are attached to ceramics molds. The standard manufacturing process of nickel superalloy castings can be improved by application of a novel insulating module for controlling the solidification process instead of standard insulating blankets.[14] Compared to standard blankets, the insulating module can be used many times in subsequent processes because it is not attached to the surface of the ceramic mold. Hence, the time and cost of manufacturing castings and subsequent utilization of ceramic waste can be reduced by removing the insulating blankets from the process. Also, the shape and method of mounting the insulation module to the mold make it possible to use other types of high-temperature insulation materials or use a different method of their production. So far, the use of the insulating module in the production of nickel superalloys castings has been tested only in laboratory conditions, where the mold with the applied thermal insulation was heated and poured in a vacuum induction furnace equipped with a preheating heater.[14] The promising results and benefits obtained encouraged the authors to test the effectiveness of the insulating module, applied instead of standard insulating blankets, during the production of castings in industrial conditions. The aim of these tests was also to develop the initial conditions for the solidification of nickel superalloy castings, enabling the replacement of the standard insulating blankets with an insulating module.

EXPERIMENT PROCEDURES AND NUMERICAL SIMULATION

Rod-shaped castings of IN 713C nickel based superalloy were produced by investment casting method in industrial conditions. Wax assemblies were the basis for manufacturing of two ceramic molds (Fig. 1b). The thermal insulating module was applied on one mold, while the other mold was left without thermal insulation; these are referenced further as the modified and standard process, respectively (Fig. 1d). The design of a cone-shaped insulation module used in the casting processes was selected based on numerical simulations of the solidification process in castings (Fig. 2). Detailed drawing of the insulating module used in these investigations is shown in Fig. 1i. The insulating module is a 215-mm-high cylinder with an outer and inner diameter of 230 and 170 mm, respectively. The outer surface of the cylinder is tilted 11°, causing the wall thickness of the insulation to expand gradually towards the gating system. There is a 114-mm-diameter hole in the top part of the module. The insulating module is an integral element built in the vacuum forming process from a mixture of fibers and both organic and inorganic binders having the following chemical composition: Al_2O_3 34 wt%, SiO_2 49 wt% and ZrO_2 17 wt%. The mold pouring cup with a slightly smaller diameter is freely inserted through the opening in the top part of the module. The top part of the module rests directly on the gating system. The size of the inner diameter of the module is matched to the shape of the ceramic to allow its easy application to the mold in a short time. This way of mounting the module leads to a gap, approximately 9 mm wide, between the outer surface of the mold (test casting zone) and the inner surface of the module (Fig. 1e). In this way, the module was not divided into smaller parts to be put on the mold, facilitating the subsequent handling of the entire assembly and heating in the furnace. The pouring cup was then attached to the mold with ceramic adhesive (Fig. 1d). Then, molds of both types were placed in the chamber furnace. All elements of the mold were simultaneously preheated to 1200 °C like in the standard production process in industrial conditions (Fig. 1f). The preheated mold together with the insulating module was placed inside vacuum induction melting furnace (VIM) on the insulation plate of the mold withdrawal system and then transferred to the melting chamber (Fig. 1a). The molten metal at 1480 °C was poured into the mold cavity, and after about 15 min the chamber was vented with air to atmospheric pressure (Fig. 1g, h).

The effectiveness of the insulating module in the casting process was determined mainly based on the assessment of microstructure and porosity on the cross sections of the rods. Two rod castings, which were made in two experiments, were selected for microscopic examination. The rods were sectioned perpendicularly at the distance of 15, 35, 57, 77, 97, 121, 142 and 165 mm from the casting base, and the cross sections were numbered 1 to 8, respectively. The surface and the cross sections of the rods were etched in the solution of the following composition: HNO_3 – 2 cm^3 + HCL – 80 cm^3 + $FeCl_3$ – 16 g + H_2O – 20 cm^3 to reveal dendrite and grain structures. The light microscope was used to take images of the microstructure at magnification of 25×. The dendritic microstructure was characterized by measuring the secondary dendrite arm spacing (SDAS) using the relationship:

$$\mathrm{SDAS} = \frac{L}{(n-1)} \tag{1}$$

where L is length and n is number of secondary dendrite branches.[15] About 20 measurements of SDAS were made on each cross section. The porosity

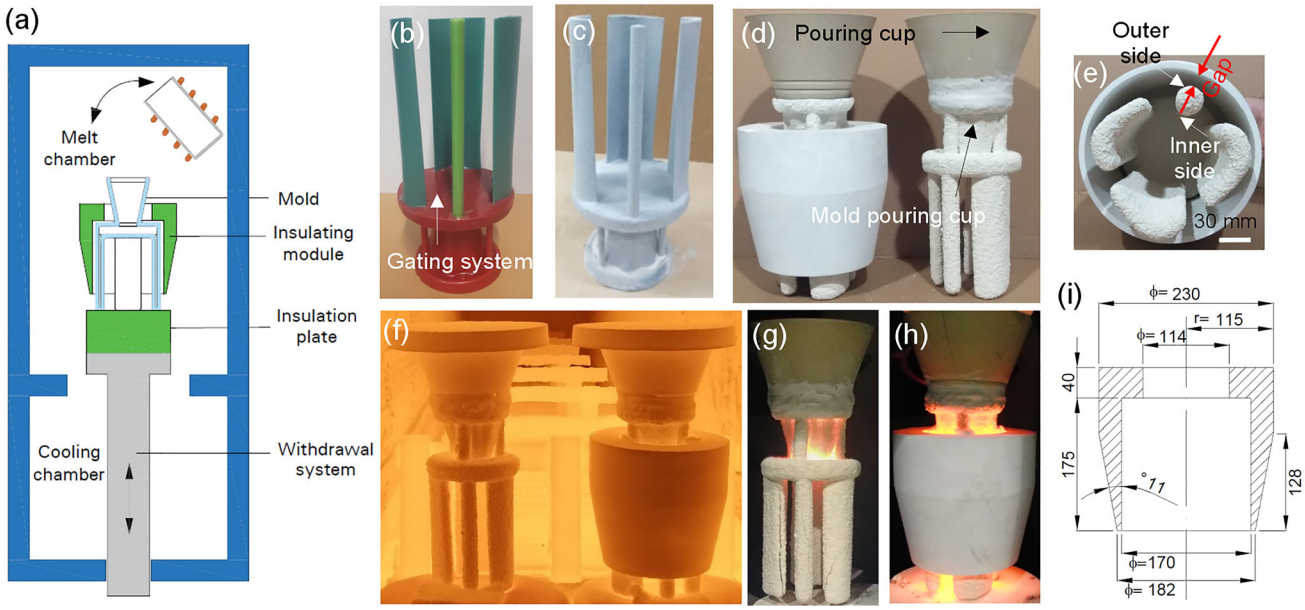

Fig. 1. Schematic illustration of vacuum induction melting furnace with the mold placed inside the melting chamber (a), wax assembly without and with prime coat of mold (b and c), mold with and without applied insulating module used in the casting trials (d), view of the mold and insulating module showing the gap between them (e), the preheating of mold inside chamber furnace (f), the mold filled with molten metal during cooling inside the furnace (g, h), the shape and dimensions of the insulating module (i).

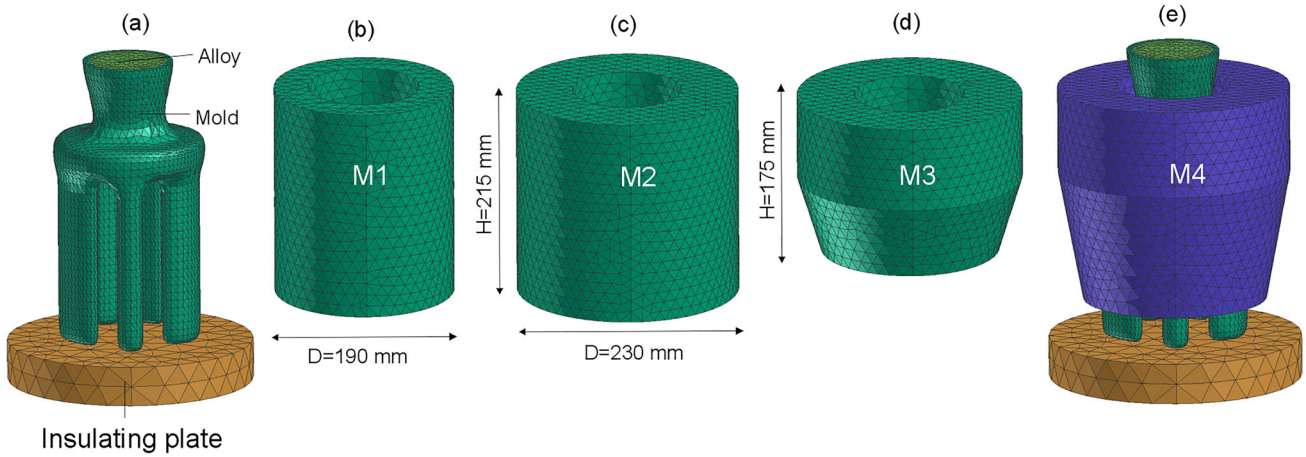

Fig. 2. Geometric model of mold with insulating plate (a) and various shapes of insulating modules: (b) M1, (c) M2, (d) M3, (e) M4.

assessment was carried out on all cross sections of the rods. Fourteen images with pores were taken at 50 × magnification on each cross section.

Numerical simulations of solidification of rod-shaped castings were carried out using ProCAST software for processes without and with different designs of the insulating module placed on mold (Fig. 2). The geometric model used in the simulation included the mold, castings, thermal insulation on which the mold was placed and insulating module. Four designs of insulating modules were analyzed, which differed in height and wall thickness inclination. The shape and dimensions of modules, labeled M1–M4 throughout the text, are shown in Fig. 2. Technological parameters such as the initial temperature of mold and alloy were assumed to be the same as in the experiments. All boundary conditions and thermophysical properties of the materials used, which were assumed for these simulations, were presented in the references.[14,15]

RESULTS AND DISCUSSION

Simulation Results

Numerical simulation of thermal and solidification conditions of castings was mainly performed to determine the optimum design of the insulating module, which will provide the formation of shrinkage porosity along the height of the rod in the acceptable range. In this way, the predicted distributions of the cooling rate, temperature gradient, *Ny* criterion and shrinkage porosity were obtained

in the cast rods (Figs. 3, 4). The boundary conditions and thermo-physical coefficients of the materials assumed in the simulations were verified experimentally by comparing the predicted cooling rates in the casting with the results obtained experimentally. The cooling rate was determined using equation:

$$v = \frac{T_L - T_S}{t_L - t_S} \quad (2)$$

where T_L and T_S are temperatures of liquidus and solidus, respectively; t_L and t_S are times required to reach the liquidus and solidus temperature in the selected points of the casting, respectively.

Application of the thermocouples in the furnace and therefore measurement of the temperature inside castings manufactured under production conditions was not possible, because the mold was transferred from the chamber furnace to the VIM furnace in a short time of about 20 s to prevent its excessive cooling. Hence, the application of the traditional numerical simulation verification method based on a comparison of the experimental and predicted cooling curves could not be used. Therefore, a method of verification of the predicted solidification parameters was developed, which considered the characteristic of the experimentally obtained dendritic microstructure. The methodology of determining the experimental cooling rate is discussed in the next section. It was found that the predicted and experimental cooling rates showed a right degree of consistency along the casting height (Fig. 3f). The analysis of results showed that the cooling rate and temperature gradient reached constant values in the height range from 40 to 140 mm for the casting produced without the use of an insulating module (Fig. 3a, g). The solidification parameters changed intensively only in the area of the casting base and the contact area of the rod with the gating system.

The use of insulating module significantly affected the solidification process. The solidification conditions for the rods varied significantly depending on the designs of M1-4 insulating modules applied. The use of M1 or M2 module with a constant wall thickness resulted in unfavorable distribution of the cooling rate and temperature gradient in terms of formation of shrinkage porosity (Fig. 3b, c, h, i). The cooling rate attained a similar value, while the temperature gradient reached the unfavorable smallest value at a height range from 80 to 140 mm in the casting with the module M1 applied on the ceramic mold. For larger wall thickness of the module (M2), the cooling rate decreased, but the temperature gradient reached the smallest value in the casting area at a height of approximately 140 mm. More favorable distribution of the solidification parameters in the upper part of the casting existed when module (M3) with variable wall thickness along its height was used (Fig. 3d, j). However, too low height of a module led to an increase in the cooling rate in the lower part of the rod. Consequently, in this area, the zone with the lowest temperature gradient was formed, as in the casting made without using thermal insulation. Hence, in the next simulation, the M4 module with a greater height and gradually changing wall thickness was used (Fig. 2e). For this design of the module, the cooling rate continuously decreased

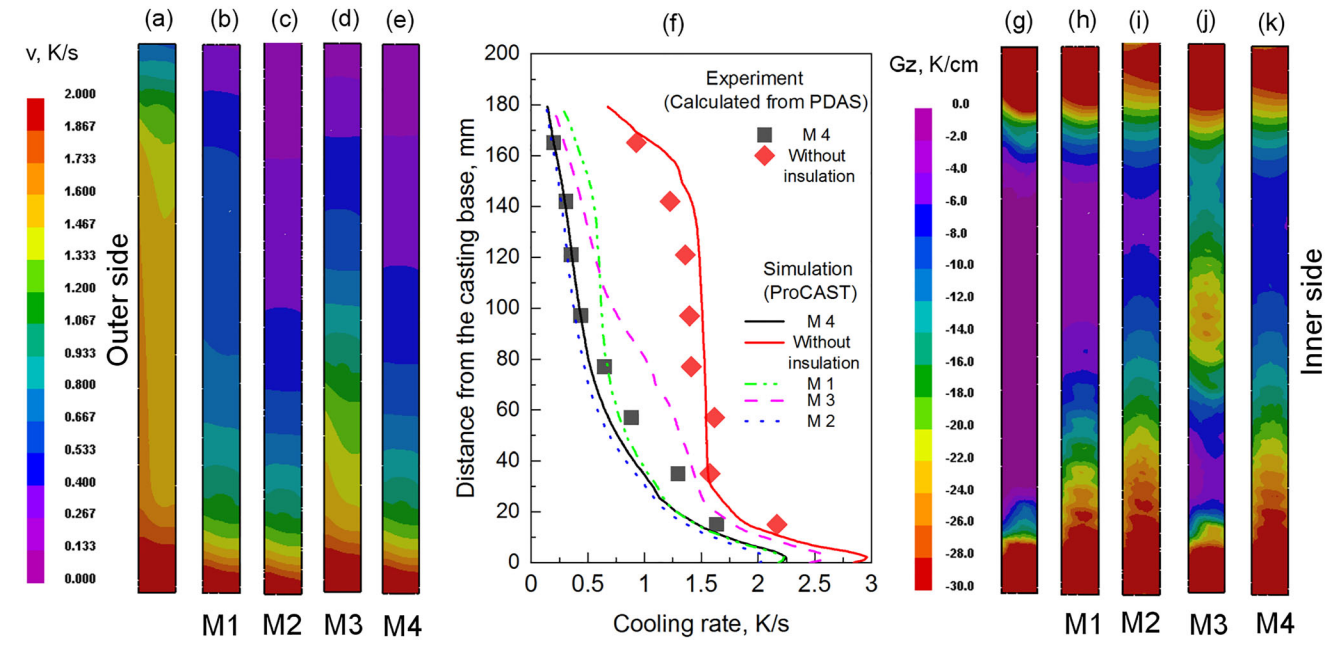

Fig. 3. Distribution of simulated cooling rate (a–e) and temperature gradient (g–k) on the longitudinal section of the rod manufactured without (a, g) and with use of various insulating modules (M1–M4) (b–e, h–k). Comparison of simulated and experimental cooling rates in the symmetry axis of the rod (f).

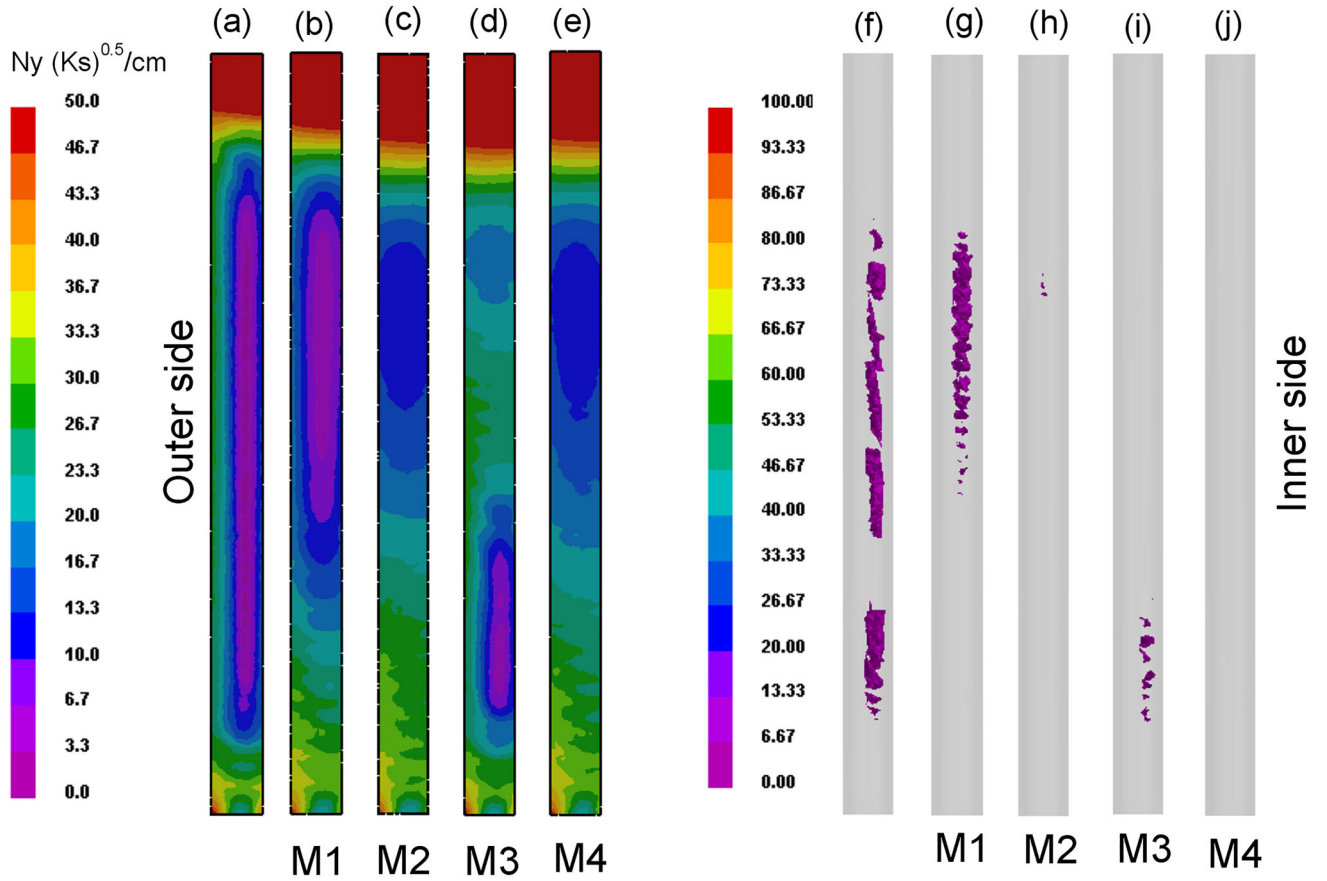

Fig. 4. Distribution of the *Ny* value (a–e) and shrinkage porosity > 2% (f–j) in rod-shaped castings manufactured without (a, f) and with the use of insulating module of various design M1–M4 (b–e, g–j).

along the rod height when the insulating module wall thickness increased (Fig. 3e, f). Such solidification conditions allowed achieving the most favorable cooling conditions of the casting, enabling directional solidification along the whole rod height.

The predicted area of shrinkage porosity formation in rod castings was determined based on the Niyama (Ny) criterion and the shrinkage porosity model of the ProCAST software (Fig. 4). The Ny value depends on the local thermal parameters such as cooling rate v and temperature gradient G, according to the relationship:[16,17]

$$Ny = \frac{G}{\sqrt{v}} \tag{3}$$

It is assumed that increasing the Ny value above a given threshold reduces the tendency to the formation of shrinkage porosity. The shrinkage porosity model is based on the knowledge of the local solid fraction contour distribution in the casting (Fig. 5). It allows to determine the location of porosity and volume fraction of pores in the casting (Fig. 4f–j). Assuming the critical value of the solid fraction for which poor feeding of interdendritic areas with liquid metal during the last stage of solidification takes place, and knowing the predicted contours of

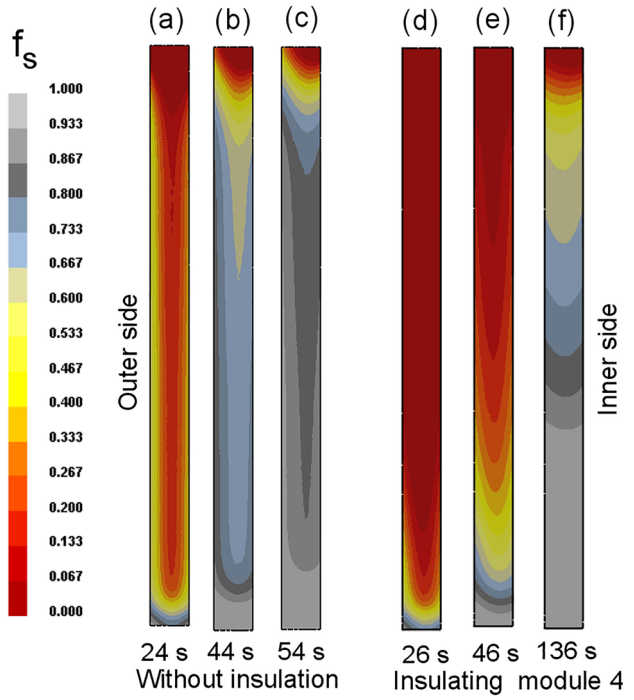

Fig. 5. Solid fraction contours at different solidification time of rod manufactured without (a–c) and with the use insulating module M4 (d–f).

the solid fraction, the areas of porosity formation in the casting are determined. The physical basis of the model used is presented in detail in Refs. 12 and 18. The simulation results showed that contours with $Ny < 10$ $(Ks)^{0.5}/cm$ were located in the area of casting where the predicted shrinkage porosity reached the value > 2% (Fig. 4). This showed that the shrinkage porosity formation was related to the local solidification parameters. The highest predicted shrinkage porosity was formed along the casting height in the area of symmetry axis when thermal insulation was not used in the process (Fig. 4a, f). The surface layer of the rod solidified first, and then the solidification front moved towards the casting axis (Fig. 5a–c). The completion of the solidification process in the middle area of the rod promoted the formation of centerline shrinkage porosity along the casting height. The use of an insulation module significantly increased the *Ny* values in selected areas of the casting (Fig. 4b-e). However, for the M1 and M3 modules, the large porosity was still present in the upper and lower parts of casting, respectively. On the other hand, the most favorable distribution of solid fraction and *Ny* values, in terms of porosity formation, was obtained for rods manufactured with the M2 and M4 modules applied. The lower part of the rod solidified first and then the solidification front gradually moved towards the gating system (Fig. 5-d–f). For the M4 module design, centerline shrinkage porosity in the casting was the lowest. Hence, the cone-shaped module (M4) was selected for the casting trial because of the promising results of the numerical simulation of solidification process and shrinkage porosity formation.

Casting Trials, Macro- and Microstructure

The casting microstructure was assessed on cross sections located at distances of 15, 35, 57, 77, 97, 121 and 142 mm from the rod base. A typical dendritic microstructure of polycrystalline nickel superalloy was detected on the etched surfaces (Fig. 6a1–b3). Dendrite morphology was characterized by measuring the secondary dendrite arm spacing (SDAS) according to the well-known relation SDAS = $L/(n-1)$. It was found that SDAS changed to a various extent along the casting height depending on whether the thermal insulation module was applied or not (Fig. 6c). A similar value of approximately 35 μm was obtained for the entire casting when thermal insulation was not applied on the mold. The use of an insulating module with a gradually changing wall thickness resulted in the change of cooling conditions of the casting. The SDAS continuously increased with increasing distance from the casting base. An obvious relationship between the SDAS in the casting and the wall thickness of the thermal insulation was found. The increase of the thickness of thermal insulation resulted in an increase of thermal resistance and thus a reduction of heat extraction from the casting trough of the mold to the cooling area of a furnace according to the relation:

$$q = \frac{\lambda}{d} \tag{4}$$

where λ is thermal conductivity, and d is thickness of insulating module.[10,15] SDAS is often related to the cooling conditions, represented, for example, by the cooling rate v, according to the relation:

$$\mathrm{SDAS} = Kv^{-n} \tag{5}$$

For the IN713C nickel superalloy, the material constants of $K = 0.42$ and $n = 0.33$ were adopted from the data determined experimentally in other studies.[14] Hence, based on dendritic microstructure characteristic obtained experimentally, after transformation this of relation the approximate average cooling rate of the casting during its solidification can be calculated using following equation (Fig. 6d):

$$v = \left(\frac{42.6}{\mathrm{SDAS}}\right)^{2.695} \tag{6}$$

The cooling rate determined in this way was the basis for the verification of a numerical simulation of rod casting solidification, manufactured using various insulating modules. The predicted cooling rates were compared with those obtained from the experiment (Fig. 3f). A good agreement between those cooling rates was found along the rod height produced without and with the use of the insulating module M4.

It should be emphasized that the inconsistency in matching the simulated values and the values obtained from the microstructure assessment may result from some simplifications adopted in the simulation and in the calculation of the cooling rate. First, the incompatibility occurs in the lower area of the casting for the height range of 20–80 mm of the rod manufactured by the process with the insulating module used (Fig. 3f). For this process, the cooling rate varies significantly between the lower and upper regions of the casting. It is well known that the thermo-physical coefficients of an alloy depend on the cooling rate. Also, the temperatures of the beginning and end of the alloy solidification process, which is used in the calculations, depend on the cooling rate of the casting. On the other hand, the values of thermo-physical coefficients of materials adopted in the geometric model are the same despite extremely different cooling rates obtained along the height of the same casting. Also, the values of $K = 0.42$ and $n = 0.33$ (previously published in Ref. 14) were determined assuming constant values of liquidus and solidus temperatures in all the experiments, despite different cooling rates of plate castings and blade airfoil.[14] Hence, the cooling rate calculated based on the dendritic microstructure in this article may slightly differ

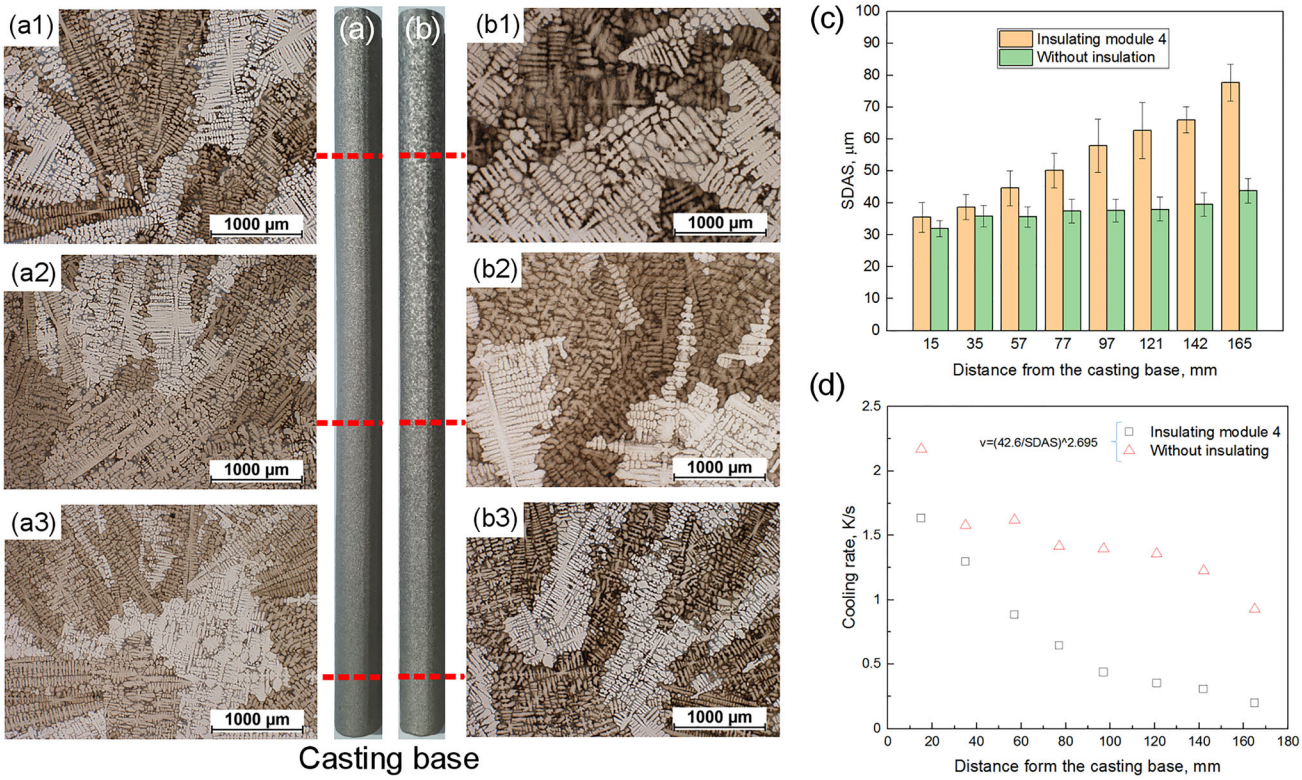

Fig. 6. Macro-etched surface of rod-shaped casting (a, b), dendrite microstructure at the cross sections 1, 4 and 7 (a1–b3) as well as SDAS along the rod height (c) manufactured without (a, a1–a3) and with (b, b1–b3) the use of insulating module, (d) cooling rate calculated from SDAS values.

from the real one. However, despite the simplifications used in the simulation and a slight inconsistency of the simulated and calculated values of the cooling rate, the effectiveness of the numerical simulation used in predicting the course of solidification process and formation of shrinkage porosity in castings manufactured under industrial conditions was proved.

An example of the grain structure on a casting surface and on its cross sections, after etching, is shown in Fig. 7. It was found that the size of equiaxed grains on the rod surface is related to the cooling conditions of the casting, in a similar way as it was for SDAS. Consequently, both the cooling rate and grain size changed in a small range along the height of the casting produced without the use of solidification control in the form of insulating module (Fig. 7a). The use of thermal insulation with varying thickness on the ceramic mold significantly changed the grain structure on the rod surface (Fig. 7b). The grain size gradually increased with increasing distance from the rod base. During the contact of the molten alloy with the inner surface of mold, its temperature dropped to the equilibrium melting point (liquidus temperature). By further reducing the temperature, the liquid melt was undercooled, which led to formation of nuclei of equiaxed grains on the inner mold surface as a result of heterogeneous nucleation.[19] It is well known that the grain density at the casting surface depends on the undercooling of the liquid melt. The amount and nucleation rate of equiaxed grain increase with increasing undercooling. In turn, the increase of cooling rate promotes the undercooling.[19,20] Hence, the grain size increased in the upper part of the casting since the use of an insulating module reduced of cooling rate in this area (Fig. 7b).

Based on the examination of casting cross section area, it was found that the grain morphology also depended on the cooling and solidification conditions of the castings. From the numerous randomly oriented grains formed on the mold surface, dendrite arms grew as a result of progressive undercooling of the adjacent region of liquid melt. As a result of the competitive growth mechanism, the grains unfavorably orientated relative to the direction of heat flow were blocked, resulting in formation of columnar grains and boundaries.[21] Columnar dendrites grew mainly from the mold surface towards the symmetry axis of the casting in the process without the use of thermal insulation (Fig. 7a1–a5). The direction of growth of these grains was approximately consistent with the direction of heat flow and coincided with the simulation of the movement of solid fraction contours (Fig. 5a–c). The lateral growth of columnar dendrites occurred, and fully columnar structure was formed almost along the whole casting height. The use of an

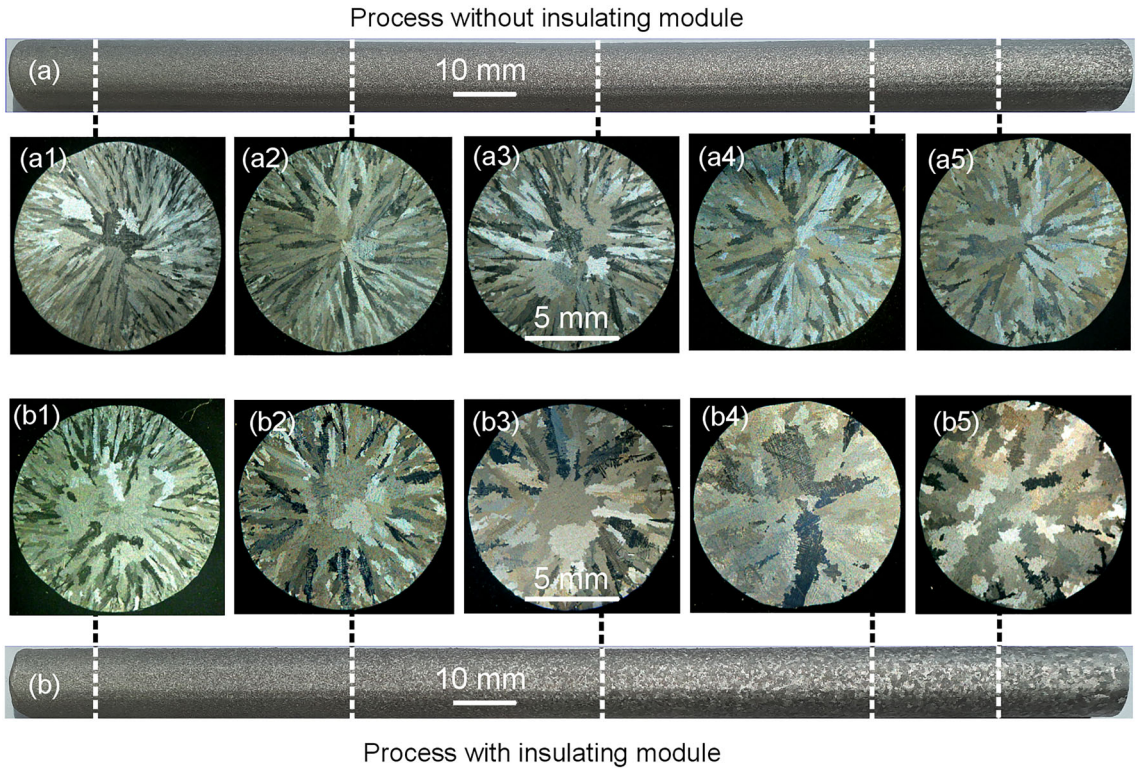

Fig. 7. An example of grain structure on the surface (a, b) and cross sections (a1–b5) of the rod casting produced without (a–a5) and with (b–b5) the use of insulating module.

insulating module totally changed the solidification conditions and thus the morphology of grain structure in the casting as well. Equiaxed grains in the center area of the rod were also formed apart from columnar grains (Fig. 7b1–b5). These equiaxed grains nucleated and grew in the undercooled liquid metal region ahead of columnar grains. The size of the columnar grain zone decreased in favor the equiaxed grains with increasing distance from the casting base. Reduction of heat extraction from the casting trough for the mold and thus decrease in both temperature gradient and cooling rate in the radial direction of the casting resulted in reduction of the extent of columnar grain zone. In this case, the heat mainly flowed in the axial direction instead of the radial one, which was also confirmed by the change in the direction of movement of solid fraction contours, promoting directional solidification of the rod (Fig. 5d–f).

Shrinkage Porosity

During manufacturing of thin-walled nickel-based superalloy precision castings, the priority is mainly to eliminate large and unfavorable centerline shrinkage porosity in castings, which can drastically reduce their mechanical properties.[22] Therefore, the proposed novel module insulating technique was mainly used to remove centerline shrinkage porosity in rods, simultaneously controlling the morphology of the dendritic microstructure and grain structure. Rod castings were radiographed to detect the actual location and estimate the amount of porosity (Fig. 8). The x-ray images show that centerline shrinkage porosity was mainly formed in the distance range of 2 to 14 cm from the rod base produced without insulating module (Fig. 8b, d, f).

Centerline shrinkage porosity was removed in the rod made using an insulating module (Fig. 8a, c, e). To confirm the x-ray inspections, the evaluation of porosity on the eight cross sections placed at the distance of 15, 35, 57, 77, 97, 121, 142 and 165 mm from the casting base was carried out using light microscopy. Figure 8c–f shows exemplary images of porosity on cross sections nos. 3 and 6 at the casting height of 56 and 121 mm, manufactured without and with insulating module. It was found that the largest shrinkage porosity was formed in the center part of the cross section.

For the quantitative assessment of porosity, the average area fraction of pores was determined on the eight cross sections placed along the rod height (Fig. 9a). For this purpose, 14 images with porosity were taken on each of them. Additionally, one image with the largest area fraction of pores (the largest porosity) was chosen from each cross section, on the basis of which the area fraction of pores in the worst field was determined (Fig. 9b).[23] The experimental results show that average area fraction of pores and their size reached much larger values in the castings without thermal insulation applied. In the

process where insulating module was applied, the porosity decreased significantly along the whole height of the casting rod (Fig. 9).

The results obtained experimentally were the basis for the verification of numerical simulation of both the location and volume fraction of pores (Figs. 4, 8, 9). Good agreement was found between the predicted areas and position of shrinkage porosity in the experimental castings. The simulation results of *Ny* value also considered the increase in porosity at the casting height of approximately 142 mm, which was produced with the insulating module applied. In this case, *Ny* attained the lowest value (Fig. 4e).

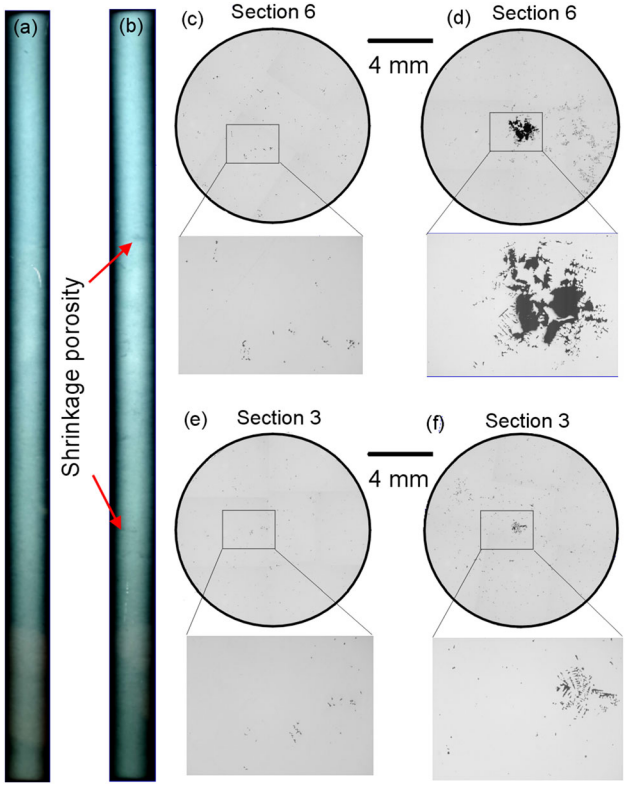

Fig. 8. X-ray images of casting rod (a, b) and exemplary images of porosity on cross sections nos. 3 and 6 at the casting height of 56 and 121 mm, manufactured without (b, d, f) and with an insulating module (a, c, e). The red arrows on the x-ray images show the position of an exemplary shrinkage porosity in the inspected rod.

The analysis of the simulation results of solid fraction contour distribution, grain morphology and size and location of pores allowed for a better understanding of the reason for the formation of the centerline shrinkage porosity and then their reduction in the casting using the insulating module technique. In the standard process, the liquid metal area, which is near the mold surface, solidified first. Then, the contours of the mushy zone moved towards the symmetry axis. This course of solidification led to the radial columnar dendrite growth and the formation of columnar grain structure almost at the whole casting height. Finally, the residual liquid metal solidified in the symmetry axis area of the rod, promoting the formation of the centerline shrinkage porosity. The location of liquidus isotherm contours and the dendrite tips created the shape of the tapered liquid feeding channel extended from the gating system towards the casting base.[2,5] From this channel, the interdendritic regions were fed by liquid metal during solidification. When the cooling rate reached similar values along the whole casting height, as it was in the process without using an insulating module, the liquid feeding channel was long and narrow. This resulted in limitation of continuous liquid metal feeding the further volumes of interdendritic areas.[6] At the last stage of solidification, the columnar dendrite growth was finished in the symmetry axis area of the rod, creating the large isolated liquid pool regions, where the liquid feeding channel

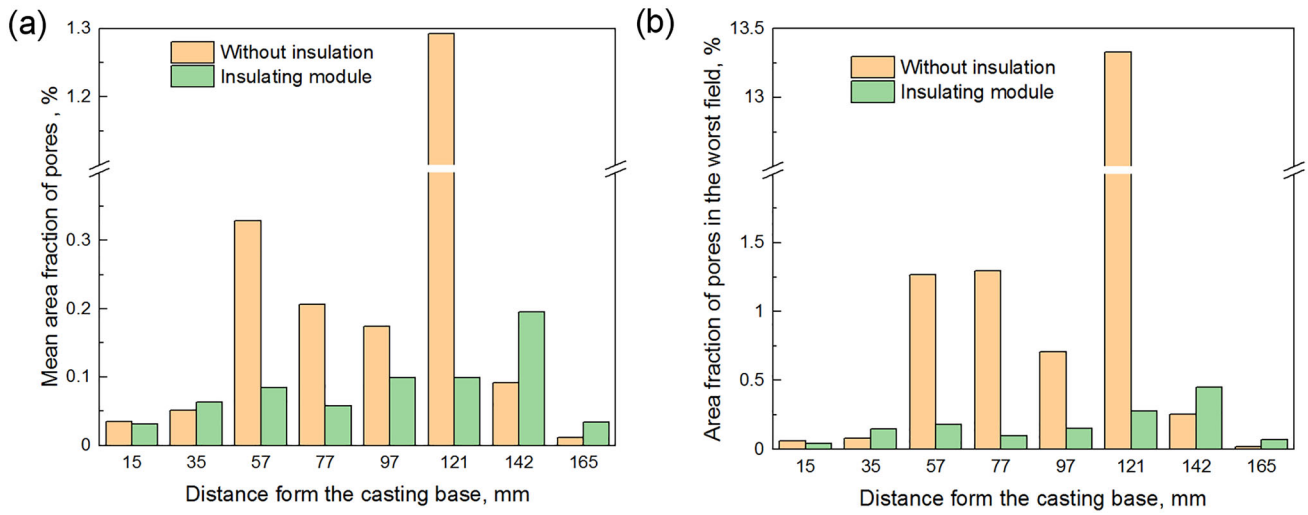

Fig. 9. Mean area fraction of pores (a) and the area fraction of pores in the worst field (b) at the cross section placed at various distances from the casting base.

existed earlier. The interdendritic regions were completely surrounded by solid; thus, the liquid metal feeding through them into the large isolated liquid pool regions was stopped, creating pore clusters during cooling of liquid metal.[9,24]

The use of thermal insulating module significantly changed the method of the solidification process of casting. The results of the numerical simulation of the solid fraction contours showed that the liquid feeding channel created gradually widened towards the gating system because of the formation of a positive temperature gradient. Its favorable widening maintained the continuous liquid metal feeding of the interdendritic regions during the solidification of the further volumes of the casting. In consequence, the large isolated liquid pool regions, which promoted the formation of pores clusters, were removed.

SUMMARY AND CONCLUSIONS

The novel insulating module technique for solidification control of Ni-based superalloy precision castings in industrial conditions has been presented in this article. Due to the promising results obtained during the numerical simulation of solidification, the design of cone-shaped insulating module M4 was chosen for solidification control, giving the largest *Ny* values and axial temperature gradient along the whole casting height. Application of the proposed insulating module on ceramic mold significantly changed the solidification process of castings compared to the process without thermal insulation. The solidification front moved from the casting base towards the gating system (directional solidification) instead of the simultaneous solidification in the whole volume of the rod produced without insulation that resulted in the unfavorable lateral growth of columnar grains and consequently centerline shrinkage porosity formation. For a predicted threshold value of $Ny > 10$ (Ks) $^{0.5}$/cm, the solidification conditions were obtained, which enabled the formation of a gradually widened liquid feeding channel along the casting height, providing a continuous liquid metal feeding of the next volumes of interdendritic areas. Consequently, shrinkage porosity clusters of the large sizes were not formed. It has been shown that the proposed insulating module technique can be successfully used to control the solidification of Ni-based superalloy castings produced in industrial conditions. Due to the possibility of using the insulating module many times, the duration and cost of the casting process can be decreased while reducing the amount of casting waste compared to the conventional investment casting process where the standard insulating blankets are attached to the mold.

ACKNOWLEDGEMENTS

This work was financed by the National Centre for Research and Development within a framework of the application project POIR.04.01.04-00-0001/17-HPT-BLADE entitled “Development of manufacturing technology of aircraft HPT gas turbine airfoil blades with internal cooling system reproduced with monolithic ceramic cores”.

CONFLICT OF INTEREST

On behalf of all authors, the corresponding author states that there is no conflict of interest.

OPEN ACCESS

This article is licensed under a Creative Commons Attribution 4.0 International License, which permits use, sharing, adaptation, distribution and reproduction in any medium or format, as long as you give appropriate credit to the original author(s) and the source, provide a link to the Creative Commons licence, and indicate if changes were made. The images or other third party material in this article are included in the article’s Creative Commons licence, unless indicated otherwise in a credit line to the material. If material is not included in the article’s Creative Commons licence and your intended use is not permitted by statutory regulation or exceeds the permitted use, you will need to obtain permission directly from the copyright holder. To view a copy of this licence, visit http://creativecommons.org/licenses/by/4.0/.

REFERENCES

1. S. Pattnaik, D.B. Karunakar, and P.K. Jha, *J. Mater. Process. Technol.* 212, 2332 (2012).
2. J. Guo, C. Beckermann, K. Carlson, D. Hirvo, K. Bell, T. Moreland, J. Gu, J. Clews, S. Scott, G. Couturier, and D. Backman, *IOP Conf. Ser. Mater. Sci. Eng.* 84, 012003 (2015).
3. G. Liu, J. SalvatCantó, S. Winwood, K. Rhodes, and S. Birosca, *Acta Mater.* 148, 391 (2018).
4. K.D. Carlson, S. Qu, and C. Beckermann, *Metall. Mater. Trans. B* 36, 843 (2005).
5. G. Sigworth, and Ch. Wang, *Metall. Mater. Trans. B* 24, 349 (1993).
6. H.S. Whitesell, and R.A. Overfelt, *Mater. Sci. Eng. A* 318, 264 (2001).
7. Z. Jie, J. Zhang, T. Huang, H. Su, Y. Li, L. Liu, W. Yang, and H. Fu, *Adv. Eng. Mater.* 18, 1785 (2016).
8. S. Zhang, Z. Xu, and Z. Wang, *Int. J. Adv. Manuf. Technol.* 91, 763 (2017).
9. L. Zheng, G. Zhang, Ch. Xiao, T.L. Lee, B. Han, Z. Li, D. Daisenberger, and J. Mi, *Scr. Mater.* 74, 84 (2014).
10. P.D. Ferro and S.B. Shendye, *Thermal analyses from thermally-controlled solidification (TCS) trials on large investment castings,* ed. R.D. Kissinger, D. J. Deye, D. L. Anton, A. D. Cetel, M. V. Nathal, T. M. Pollock and D. A. Woodford (The Minerals, Metals and Materials Society, 1996) pp. 561.
11. D. Szeliga, K. Kubiak, W. Ziaja, and R. Cygan, *Int. J. Cast Met. Res.* 27, 146 (2014).
12. A.J. Torroba, O. Koeser, L. Calba, L. Maestro, E. Carreño-Morelli, M. Rahimian, S. Milenkovic, I. Sabirov, and J. Lorca, *Integr. Mater. Manuf. Innov.* 3, 1–25 (2014).
13. D. Pieczaba, A. Jach, E. Guzik, and J. Sieniawski, *Arch. Metall. Mater.* 55, 37 (2010).
14. D. Szeliga, *J. Mater. Process. Technol.* 278, 116503 (2020).
15. D. Szeliga, K. Kubiak, W. Ziaja, R. Cygan, J.Sz. Suchy, A. Burbelko, W.J. Nowak, and J. Sieniawski, *Exp. Therm. Fluid Sci.* 87, 149 (2017).

16. E. Niyama, T. Uchida, M. Morikawa, and S. Saito, *Int. Cast Met. J.* 7, 52 (1982).
17. K.D. Carlson, and C. Beckermann, *Metall. Mater. Trans. A* 40, 163 (2009).
18. C. Pequet, M. Rappaz, and M. Gremaud, *Metall. Mater. Trans. A* 33, 2095 (2002).
19. J.A. Danzig, and M. Rappaz, *Solidification*, 1st edn. (EPFL Press, Lausanne, 2009), pp429–473.
20. J. Nawrocki, M. Motyka, D. Szeliga, W. Ziaja, R. Cygan, and J. Sieniawski, *J. Manuf. Process.* 49, 153 (2020).
21. Y.Z. Zhou, A. Volek, and N.R. Green, *Acta Mater.* 56, 2631 (2008).
22. L. Kunz, P. Lukáš, R. Konečná, and S. Fintová, *Int. J. Fatigue* 41, 47 (2012).
23. S. Roskosz, M. Staszewski, and J. Cwajna, *Mater. Charact.* 56, 405 (2006).
24. E. Plancher, P. Gravier, E. Chauvet, J.-J. Blandin, E. Boller, G. Martin, L. Salvo, and P. Lhuissier, *Acta Mater.* 181, 1 (2019).

Publisher's Note Springer Nature remains neutral with regard to jurisdictional claims in published maps and institutional affiliations.